Available online at www.sciencedirect.com
SCIENCE DIRECT®
Bioorganic & Medicinal Chemistry Letters
Bioorganic & Medicinal Chemistry Letters 16 (2006) 2000–2007

Synthesis and structure–activity relationship of 3,4′-bispyridinylethylenes: Discovery of a potent 3-isoquinolinylpyridine inhibitor of protein kinase B (PKB/Akt) for the treatment of cancer

Qun Li,[a,*] Keith W. Woods,[a] Sheela Thomas,[a] Gui-Dong Zhu,[a] Garrick Packard,[a] John Fisher,[a] Tongmei Li,[a] Jianchun Gong,[a] Jurgen Dinges,[a] Xiaohong Song,[a] Jason Abrams,[a] Yan Luo,[a] Eric F. Johnson,[a] Yan Shi,[a] Xuesong Liu,[a] Vered Klinghofer,[a] Ron Des Jong,[b] Tilman Oltersdorf,[b] Vincent S. Stoll,[a] Clarissa G. Jakob,[a] Saul H. Rosenberg[a] and Vincent L. Giranda[a]

[a]*Cancer Research, GPRD, Abbott Laboratories, Abbott Park, IL 60064-6101, USA*
[b]*Idun Pharmaceuticals, 9380 Judicial Dr., San Diego, CA 92121, USA*

Received 29 November 2005; revised 15 December 2005; accepted 19 December 2005
Available online 18 January 2006

Abstract—Structure-based design and synthesis of the 3,4′-bispyridinylethylene series led to the discovery of 3-isoquinolinylpyridine **13a** as a potent PKB/Akt inhibitor with an IC_{50} of 1.3 nM against Akt1. Compound **13a** shows excellent selectivity against distinct families of kinases such as tyrosine kinases and CAMK, and displays poor to marginal selectivity against closely related kinases in the AGC and CMGC families. Moreover, **13a** demonstrates potent cellular activity comparable to staurosporine, with IC_{50} values of 0.42 and 0.59 μM against MiaPaCa-2 and the Akt1 overexpressing FL5.12-Akt1, respectively. Inhibition of phosphorylation of the Akt downstream target GSK3 was also observed in FL5.12-Akt1 cells with an EC_{50} of 1.5 μM. The X-ray structures of **12** and **13a** in complex with PKA in the ATP-binding site were determined.

Kinase inhibitors have generated considerable interest due to the remarkable success of Gleevec and other inhibitors of tyrosine kinases (TKs) in clinical oncology.[1] As one of the major downstream targets of several receptor TKs in the signal transduction pathways, Akt (PKB) plays a central role in promoting cancer cell proliferation and survival.[2] Akt is a serine/threonine kinase belonging to the AGC family of kinases.[3] It is overexpressed and constitutively activated in a large number of human tumors.[2f] Antisense inhibition of Akt has been shown to inhibit proliferation and induce apoptosis in several cancer cells.[4] All of these findings have recently led to an intense search for small molecule inhibitors of Akt as anticancer agents.[5] In the preceding paper,

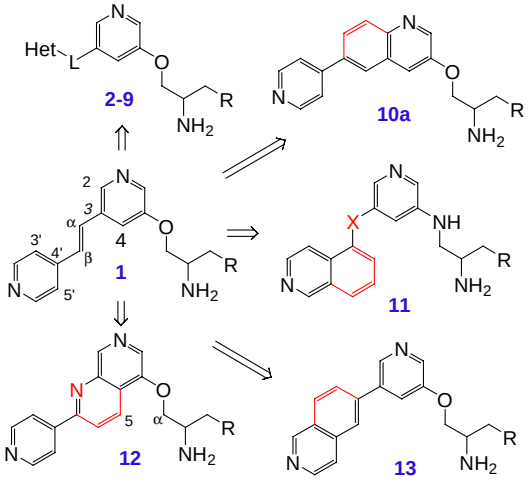

Figure 1. Modifications of **1** yielded potent Akt inhibitor (**13**).

Keywords: Inhibitors of Akt; Akt1; Akt2; Akt3; PKA; PKB; protein kinase B; GSK3; FL5.12-Akt1; X-ray; Anticancer; Apoptosis; Antitumor; Pharmacokinetics; Kinase inhibitors; Structure-based design.
* Corresponding author. Tel.: +1 847 937 7125; fax: +1 847 936 1550; e-mail: qun.li@abbott.com

0960-894X/$ - see front matter © 2005 Elsevier Ltd. All rights reserved.
doi:10.1016/j.bmcl.2005.12.065

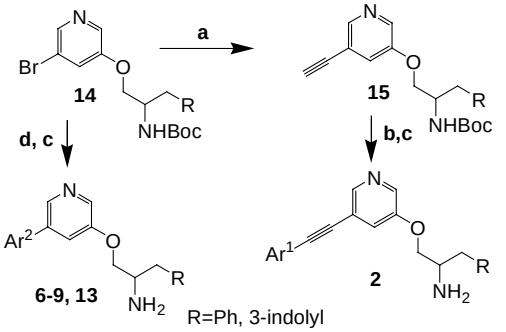

Scheme 1. Reagents and conditions: (a) i—TMSC≡CH, CuI/$Pd_2Cl_2(PPh_3)_2$, Et_3N, DMF, 50 °C, 15 h, 80%; ii—TBAF, THF, rt, 86%; (b) Ar^1Br, CuI/$Pd_2Cl_2(PPh_3)_2$, Et_3N, DMF, 50 °C, 20 h, 60–75%; (c) TFA, CH_2Cl_2, rt, 2 h; (d) Ar^2SnMe_3, $Pd_2(dba)_3$/P(*o*-tol)$_3$, DMF, 75 °C, 8 h, or $Ar^2B(OH)_2$, $Pd(PPh_3)_4$, DMF, 100 °C, 8–10 h or i—$Me_3SnSnMe_3$, $Pd(PPh_3)_4$, toluene, 100 °C, 8 h; ii—Ar^2Br, $Pd_2(dba)_3$/P(*o*-tol)$_3$, DMF, 75 °C, 8 h.

we reported a novel series of Akt inhibitors that contain the 3,4′-bispyridinylethylene core (**1**) resulting from structural modifications of a screening lead.[6] We report herein our continued optimization efforts of the 3,4′-bispyridinylethylene series that has led to the identification of 3-isoquinolinylpyridine **13a** as a potent PKB/Akt inhibitor with an IC_{50} of 1.3 nM against Akt1 (Fig. 1).

Syntheses of the alkyne (**2**) and 3-arylsubstituted pyridines **6**–**9** and **13** are outlined in Scheme 1. Sonogashira coupling of **14**[6] with TMS-acetylene followed by deprotection of the TMS group with TBAF produced acetylene **15**, which underwent the Heck reaction with selected aryl bromides to give **2**. Conversion of **14** to the 3-arylpyridines (**6**–**9** and **13**) proceeded via the Stille or Suzuki reactions with corresponding tin or boronic acid coupling partners.

The analogs (**3**–**5** and **7**) with double bond replacements were prepared as described in Scheme 2. Amide **3** was prepared in a three-step sequence involving palladium-catalyzed carboxylation of **14**, coupling of the resulting **16** with 4-aminopyridine and deprotection with TFA. Palladium-catalyzed amination of bromide **14** with benzophenone imine following the procedure developed by Buchwald et al.,[7] and subsequent acid hydrolysis provided amine **17**. Coupling of **17** with pyridinecarboxylic acids in the presence of EDC and subsequent deprotection of the Boc group with TFA afforded amide **4**. Conversion of amine **17** to pyridinylmethylamine **5** was achieved through reductive amination of pyridine-carbaldehydes and subsequent TFA deprotection. Pd-catalyzed amination of bromide **14** followed by deprotection furnished compound **7**.

Preparation of the conformationally constrained analogs is illustrated in Schemes 3–5. Compound **10** with C-β of the double bond cyclized with C-2 of the central pyridine was synthesized as depicted in Scheme 3. Bromoisatin **19** reacted with bromopyruvic acid **20** in aqueous KOH solution to form the cinchoninic acid, which underwent decarboxylation in refluxing nitrobenzene[8] to provide bromohydroxy-quinoline **21**. Synthesis of

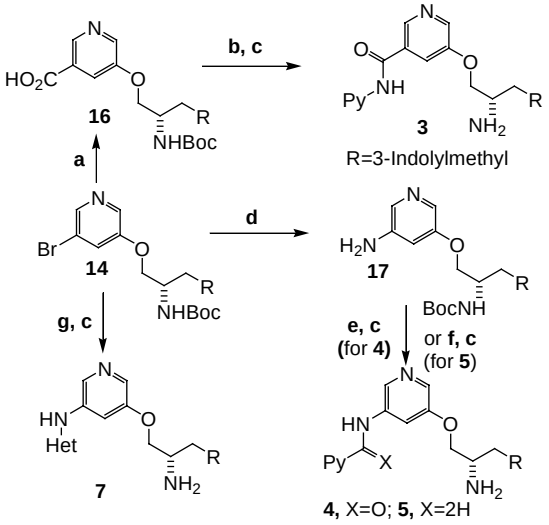

Scheme 2. Reagents and conditions: (a) CO (900 psi), $Pd(dppf)Cl_2$, THF/water, 100 °C, 19 h, 76%; (b) $PyNH_2$, EDC, HOBt, DMF, rt, overnight, 18–23%; (c) TFA, CH_2Cl_2, rt, 2 h; (d) i—$Ph_2C{=}NH$, $Pd_2(dba)_3$, BINAP, $NaOBu^t$, toluene, 80 °C, 4 h; ii—10% HCl, THF, rt, 2 h, 70%; (e) $PyCO_2H$, EDC, HOBt, DMF, rt, 50–70%; (f) PyCHO, acetic acid, MeOH, rt, 1 h; then $NaBH_3CN$, rt, 1 h, 70%; (g) *t*-BuONa, $Pd_2(dba)_3$, dioxane, 90 °C, 3 h, 60–75%.

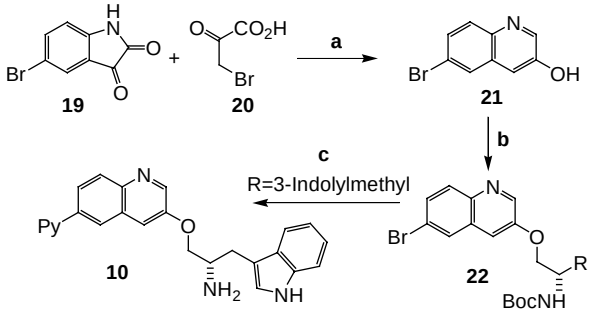

Scheme 3. Reagents and conditions: (a) i—KOH, water, rt, 6 days, 58%; ii—nitrobenzene, reflux, 5 min, 55%; (b) *N*-Boc-L-tryptophanol, DEAD/PPh_3, THF, rt, 2 h, 72%; (c) i—$PyB(OH)_2$, $Pd(PPh_3)_4$, DMF, 100 °C, 8 h, 70–76%; ii—TFA, CH_2Cl_2, rt, 2 h, 90%.

10 from **21** was carried out using the same three-step protocol as described in Scheme 1.

Ullmann coupling between dibromopyridine **23a** and phenol **24a** at 240 °C under microwave conditions gave ether **25a**. Palladium-catalyzed amination of aminopyridine **23b** with triflate **24b** provided aniline **25b**. Compounds **25a**–**b** were converted to amines **26** as previously described followed by acid hydrolysis. Reductive amination of **26** with *N*-Boc-tryptophanal in the presence of $NaBH_3CN$ and Ti(*i*-PrO)$_4$ and subsequent acidic deprotection of the Boc group provided compounds **11a**–**b** (Scheme 4).

Preparation of analogs cyclized between C-β and C-4 of the central pyridine is shown in Scheme 5. PMB protected bromopyridine **27b** (made from **27a**) was converted to 3-Boc-aminopyridine **28** via the amination protocol as previously described followed by Boc protection in

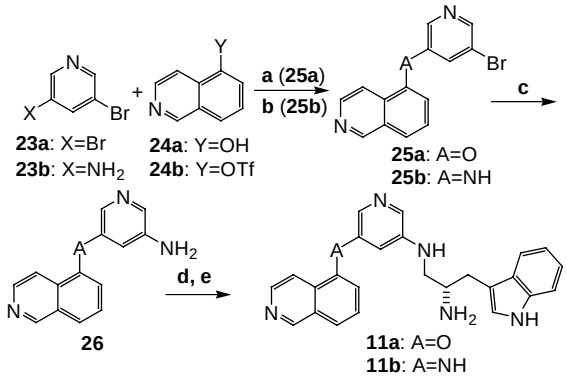

Scheme 4. Reagents and conditions: (a) **23a** + **24a**, K_2CO_3, DMF, microwave, 240 °C, 10 min, 23%; (b) **23b** + **24b**, $Pd_2(dba)_3$, BINAP, NaOBu′, DMF, 90 °C, 8 h, 18%; (c) i—$Ph_2C{=}NH$, $Pd_2(dba)_3$, BINAP, NaOBu′, toluene, 80 °C, 3 h; ii—1 N HCl, THF, rt, 15 min, 44–45%; (d) *N*-Boc-L-tryptophanal, $Ti(i\text{-}PrO)_4$, CH_2Cl_2, 2 h; then $NaBH_3CN$, 2 h, 24–40%; (e) TFA, CH_2Cl_2, rt, 2 h.

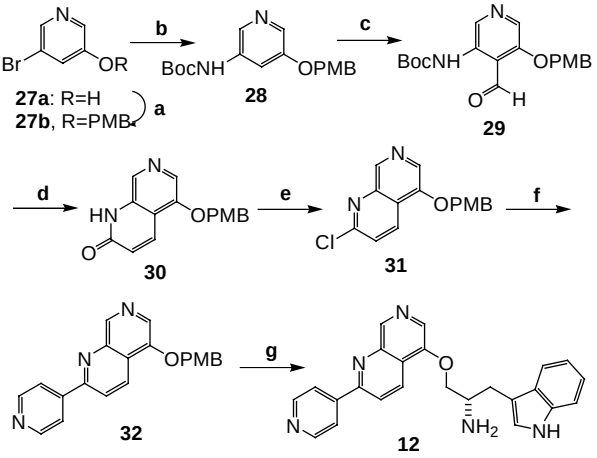

Scheme 5. Reagents and conditions: (a) PMBCl, K_2CO_3, Bu_4NCl, DMF, rt, 3.5 days, 50%; (b) i—$Ph_2C{=}NH$, $Pd_2(dba)_3$, BINAP, NaOBu′, toluene, 80 °C, 3 h; ii—1 N HCl, THF, rt, 15 min, 71%; iii—Boc_2O, $KN(TMS)_2$, THF, rt, 55%; (c) BuLi, HCO_2CH_3, −78–10 °C, 45 min, 63%; (d) i—$(CF_3CH_2O)_2POCH_2CO_2CH_3$, $KN(TMS)_2$, THF, −78 °C, 20 min; ii—$NaN(TMS)_2$, rt, 30 min, 75%; (e) $POCl_3$, DMF, 45 °C, 6 h, 79%; (f) 4-$PySnBu_3$, $Pd_2(dba)_3$, Cy-MAP1, Et_3N, DMF, 100 °C, 5 h, 49%; (g) i—1 N HCl, EtOH, 90 °C, 2 h, 74%; ii—*N*-Boc-L-tryptophanol, DEAD, PPh_3, THF, rt, 4 h, 83%; iii—TFA, *p*-methoxythiobenzyl alcohol, CH_2Cl_2, rt, 20 min, 60%.

the presence of $KN(TMS)_2$. Lithiation of **28** with *n*-BuLi at −78 °C and subsequent quenching of the anion with methyl formate afforded aldehyde **29**. Wittig–Horner reaction of aldehyde **29** with methyl bis(trifluoroethyl)phosphonoacetate and cyclization with $NaN(TMS)_2$ provided **30**. 2-Naphthyridone **30** was converted to chloride **31** by $POCl_3$ in DMF followed by coupling with 4-tributylstannylpyridine to provide **32**. Compound **32** was treated with HCl to remove the PMB group and the resulting phenol was coupled to Boc-tryptophanol via the Mitsunobu reaction. Finally, acidic deprotection of the Boc group yielded **12**.

The X-ray structure of **1b** in complex with PKA[6] (a kinase closely related to Akt) revealed that the nitrogen of the terminal pyridine binds to the hinge region via a hydrogen bond with the backbone NH of Val123, while the nitrogen of the central pyridine hydrogen bonds to the amino group of Lys72. Although the terminal pyridine is tightly sandwiched between the isopropyl group of Leu173 and the methyl group of Ala70, there is available space surrounding the *trans*-double bond linking the two pyridines. Therefore, our initial efforts focused on replacing the double bond with other functional groups (Table 1). Substitution of the double bond with a triple bond (**2a**) resulted in sharply lowered activity. The lost activity in linear acetylene **2a** cannot be regained with an angled 3-pyridinyl group (**2b**). The bioisosteric amide analogs (**3a**, **4a**–**b**) are much less active than the corresponding double bond analogs (**1a**–**b**). These results are consistent with the highly hydrophobic nature of the binding pocket. All other double bond replacements including the methylamine (**5a**–**b**), amine (**7a**–**d**) *ortho*-phenyl (**6a**), and 2,4-thiazole (**6b**–**c**) groups (Table 1) resulted in a significant loss in activity.

Bispyridine **8a** (Table 1), which has the double bond deleted, shows better than expected activity. Its IC_{50} value of 260 nM is respectable considering that the pyridine is further away from the hinge. A series of 3-arylpyridines were therefore prepared with functional groups capable of hydrogen bonding attached to the aryl rings (Table 2). Some of these compounds should presumably fit in the binding pocket better than **8a** and an additional hydrogen bond with the hinge is therefore possible. Unfortunately, none of the compounds in Table 2 shows improved activity to **8a**, except for **9m**, which has an IC_{50} of 227 nM. We speculate that the lack of van der Waals interactions with Ala70 and Leu173 for these analogs (**9a**–**x**), as seen for **1b**, may contribute partially to the poor activity.

Having been unsuccessful in replacing the *trans*-double bond, we next investigated structures resulting from cyclizations of the *trans*-double bond onto the adjacent pyridines. This approach also restricts the number of rotatable bonds and hence has the potential to increase potency. As shown in Figure 1, there are four possible ways to cyclize the double bond onto either the central or terminal pyridine. Note that in the X-ray structure in complex with PKA, **1** adopts the conformation shown in Figure 1. In order to cyclize C-β with C-2 (**10a**), the single bond connecting C-α has to rotate 180° to a less favorable conformation. The resulting analog **10a** is 21-fold less active than **1b** (Table 3). Replacing the 4-pyridine moiety in **10a** with a 3-pyridine imparts an additional 24-fold drop in activity (**10b**). Activity also decreased sharply for analogs **11a**–**b** incorporating cyclizations between C-β and C-5′. Cyclization between C-β and C-4 appears to be more favorable. The resulting naphthyridine (**12**) shows improved potency as compared with compounds **10** and **11**, but is still 14-fold less potent than **1b**. Finally, cyclization between C-α and C-3′ led to a breakthrough Akt1 inhibitor **13a**, which is 10-fold more potent than **1b** with an IC_{50} of 1.3 nM. Compound **13a** possesses one less rotatable bond than **1b**, and it contains an isoquinoline group that provides stronger van der Waals interactions with the hydropho-

Table 1. Activity of Akt inhibitors[a]

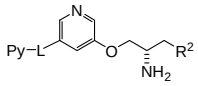

Compound	Py	L	R^2	Akt1 IC_{50}[a] (nM)
1a				690
1b				14
2a				210
2b				25,200
3a				2020
4a				31,950
4b				26%[b]
5a				26%[b]
5b				41%[b]
6a				10%[b]
6b				9870
6c				9350
7a				2860
7b				2160
7c				18,830
7d				6970
8a		Bond		260

[a] Against Akt1 with ATP concentration of 10 μM.[6]
[b] Inhibition at 50 μM.

bic pocket than does the vinylpyridinyl group in **1b**. Note that *S*-isomer **13a** is 20-fold more potent than the corresponding *R*-isomer **13b**.

The selectivity profile and cellular activity of **13a** and **1b**[6] are summarized in Table 4. The non-selective kinase inhibitor staurosporine was used as a control.

Table 2. Activity of Akt inhibitors[a]

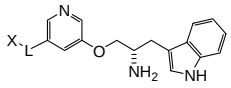

Compound	X	L	Akt1 IC_{50}[a] (nM)
9a		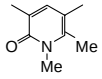	1340
9b			1830
9c			1560
9d			13%[b]
9e			6940
9f			31,280
9g			9310
9h			41%[b]
9i			48%[b]
9j			12%[b]
9k			0%[b]
9l			1390
9m			227
9n			12,030
9o			3%[b]
9p			33,010
9q			33,160
9r	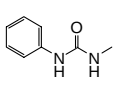		1120

Table 2 (*continued*)

Compound	X	L	Akt1 IC_{50}[a] (nM)
9s			2710
9t			14,330
9u			3670
9v			6230
9w	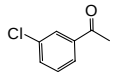	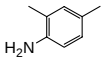	1450
9x			2170

[a] Against Akt1 with ATP concentration of 10 μM.[6]
[b] Inhibition at 50 μM.

Table 3. Activity of Akt inhibitors[a,b]

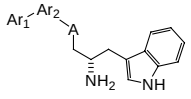

Compound	Ar_1	Ar_2	A	Akt1 IC_{50}[a] (nM)
10a		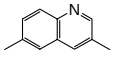	O	300
10b		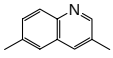	O	7090
11a			NH	210
11b			NH	270
12			O	190
13a (*S*-)			O	1.3
13b (*R*-)			O	26

[a] Unless otherwise specified, all compounds are *S*-enantiomers.
[b] Against Akt1 with ATP confcentration of 10 μM.[6]

Overall, compound **13a** demonstrates excellent selectivity against distinct families of kinases including TK and CAMK,[3] and possesses IC_{50} values greater than 5 μM against most of these kinases. However, selectivity against closely related kinases of the AGC[3] and CMGC[3] families is poor to moderate because of the high degree of homology in the ATP-binding pocket. Similar to **1b**, **13a** largely displays no selectivity for any of the three Akt isoforms, presumably due to very high sequence homology, especially in the ATP-binding pocket where the homology is nearly 100% (except one non-crucial amino acid in Akt3). For similar reasons, **13a** is non-selective against PKA (IC_{50} = 2.1 nM). Selectivities versus other closely related kinases such

Table 4. Selectivity profile and cellular activity of **1b** and **13a** in comparison with those of staurosporine (IC_{50},[a] nM)

Test	Name	**1b**	**13a**	Staurosporine
Kinases	Akt1	14	1.3	1.5
	Akt2	257	6.8	6.5
	Akt3	354	35	10
	PKA	38	2.1	3.6
	PKCγ	1200	270	6.6
	PKCζ	930	6100	570
	CDK1	>10,000	100	0.4
	ERK2	12,850	910	370
	MAPK-AP2	>10,000	>50,000	110
	CK2	>50,000	11,800	3400
	Chk1	16,000	4200	9.5
	KDR	>50,000[b]	>50,000[b]	88[b]
	FLT4	>50,000[b]	>50,000[b]	58[b]
	C-KIT	>50,000[b]	26,200[b]	23[b]
	SRC	>50,000[b]	>50,000[b]	1920[b]
Cellular activity[6]	GSK3-P[c]	10,000	1500	460
	FL5.12-Akt1 (MTT)[d]	3000	420	290
	MiaPaCa-2 (MTT)[d]	12,000	590	370

[a] Unless otherwise specified, ATP concentration at 10 μM.[6]
[b] ATP concentration at 1.0 mM.
[c] EC_{50} against GSK3 phosphorylation in the Akt1 overexpressing cell FL5.12-Akt1.
[d] IC_{50} against cell proliferation in MTT assays.

as PKC, CDK, and ERK2 are moderate, ranging from 77- to 500-fold.

Compound **13a** was evaluated for its antiproliferative activity against FL5.12-Akt1 murine prolymphocytic cells that overexpress Akt1 and MiaPaCa-2 human pancreatic cancer cells.[6] Its IC_{50} values of 0.42 and 0.59 μM against the Akt1 overexpressing FL5.12-Akt1 and MiaPaCa-2, respectively, represent approximately a 10-fold improvement over **1b**, and are comparable with that of staurosporine (Table 4). These improvements in cellular potency for **13a** are in agreement with the same comparable increases in enzymatic activity observed relative to **1b**. Compound **13a** also inhibits the phosphorylation of the Akt downstream target GSK3 in FL5.12-Akt1 cells with an EC_{50} of 1.5 μM.[6]

The X-ray structures of **12** and **13a** in complex with PKA in the ATP-binding site have been determined (Fig. 2).[9] The binding pattern of **13a** is almost identical to that of**1b**.[6] The nitrogen of the isoquinoline binds to the hinge via a hydrogen bond with the backbone NH of Val123 with a distance of 3.0 Å between the two nitrogens. The pyridine of the isoquinoline is sandwiched between the isopropyl group of Leu173 and the methyl group of Ala70, while the benzene ring of the isoquinoline is in a

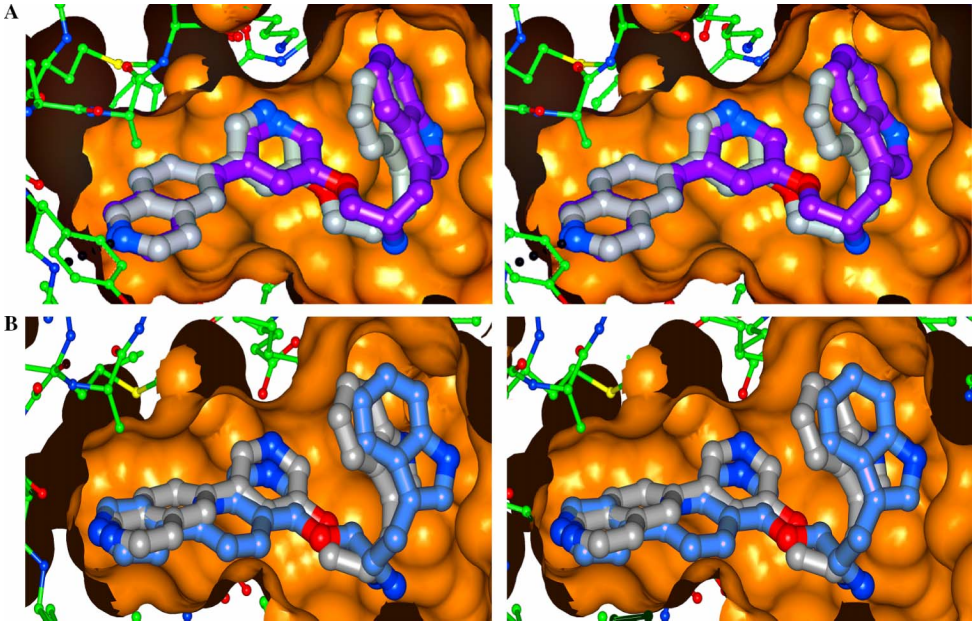

Figure 2. Stereo views of overlays of X-ray structures[9] of Akt inhibitors **13a** (in gray) and: (A) **1b** (in purple); (B) **12** (in blue) in complex with PKA in the ATP-binding site.

hydrophobic pocket defined by amino acid residues of Val57, Ala70, Val104, Met120, Leu173, and Thr183. C-1 of the isoquinoline is buried deep inside the binding cavity with a distance of merely 3.2 Å between C-1 and the carbonyl group of Glu121, leaving little space for any group larger than hydrogen atom. Interestingly, if the C-1 hydrogen of the isoquinoline were capable of hydrogen bonding, it might be a perfect fit. The nitrogen of the central pyridine hydrogen bonds to the amino group of Lys72 (distance between the nitrogens is 2.8 Å). The charged primary amine of the side chain sits tightly in the Mg-binding loop, binding to Asn171 and Asp184 via H-bonds and ionic interactions. The indole ring packs underneath the glycine-rich loop with an average distance of 3.5 Å to the loop. Note that the entrance to the ATP-binding pocket near the hinge region is partially blocked by residues 315–327 of the C-terminal domain. The nearest distance from the isoquinoline to Phe327 is approximately 3.5 Å, enabling the isoquinoline of **13a** to fit tightly in the hinge region.

Overlay of structures of **12** and **13a** (Fig. 2b) in complex with PKA revealed that **12** binds similarly to **13a**, except that the side chain of **12** is forced into an unfavorable position due to the clash between H-5 of the isoquinoline and H-α of the side chain (Fig. 1). This change leads to weakened hydrogen bonding interactions of the primary amino group with Asn171 and Asp184. The distances of the hydrogen bonds are in sub-optimal lengths of 3.4 and 4.1 Å, respectively. In comparison, the primary amino group of **13a** is positioned 2.9 Å equally from the above residues.

In summary, structure-based design and synthesis of the 3,4′-bispyridinylethylene series of Akt/PKB inhibitors led to the discovery of 3-isoquinolinylpyridine **13a**, which exhibits an IC_{50} of 1.3 nM against Akt1. Compound **13a** shows excellent selectivity against distinct families of kinases such as TK and CAMK, and displays poor to marginal selectivity against closely related kinases in the AGC and CMGC families. Moreover, **13a** demonstrates potent cellular activity comparable to staurosporine. Inhibition of the phosphorylation of the Akt downstream target GSK3 by **13a** was also observed in FL5.12-Akt1 cells. With the available X-ray structures of the Akt inhibitors in complex with PKA, further structural refinements of this series via structure-based design to optimize the physiochemical and biological properties of molecules is ongoing, the results of which will be published in due course.[10]

Acknowledgments

The authors are grateful to Mr. Rick Clark, Dr. Moshe Weitzberg, Dr. Matt Hensen, Dr. Robert Keyes, Dr. Curt Cooper, and Dr. Chris Krueger for proofreading and valuable suggestions. X-ray crystallographic data were collected at beamline 17-ID in the facilities of the Industrial Macromolecular Crystallography Association Collaborative Access Team (IMCA-CAT) at the Advanced Photon Source, which are supported by the companies of the Industrial Macromolecular Crystallography Association.

References and notes

1. (a) Druker, B. J. *Adv. Cancer Res.* **2004**, *91*, 1; (b) Krause, D. S.; Van Etten, R. A. *N. Engl. J. Med* **2005**, *353*, 172; (c) Ross, J. S.; Schenkein, D. P.; Pietrusko, R.; Rolfe, M.; Linette, G. P.; Stec, J.; Stagliano, N. E.; Ginsburg, G. S.; Symmans, W. F.; Pusztai, L.; Hortobagyi, G. N. *Am. J. Clin. Pathol.* **2004**, *122*, 598.
2. For recent reviews on Akt see: (a) Barnett, F. S.; Bilodeau, M. T.; Lindsley, C. W. *Curr. Top. Med. Chem.* **2005**, *5*, 109; (b) Bellacosa, A.; Kumar, C. C.; Di Cristofano, A.; Testa, J. R. *Adv. Cancer. Res.* **2005**, *94*, 29; (c) Mitsiades, C. S.; Mitsiades, N.; Koutsilieris, M. *Curr. Cancer Drug Targets* **2004**, *4*, 235; (d) Gills, J. J.; Dennis, P. A. *Expert Opin. Investig. Drugs* **2004**, *13*, 787; (e) Vivanco, I.; Sawyers, C. L. *Nat. Rev. Cancer* **2002**, *2*, 489; (f) Li, Q.; Zhu, G.-D. *Curr. Top. Med. Chem.* **2002**, *2*, 939.
3. Hanks, S.; Hunter, T. *FASEB* **1995**, *9*, 576.
4. (a) Liu, X.; Shi, Y.; Han, E. K.; Chen, Z.; Rosenberg, S. H.; Giranda, V.; Luo, Y.; Ng, S. C. *Neoplasia* **2001**, *3*, 278; (b) Cheng, J. Q.; Ruggeri, B.; Klein, W. M.; Sonoda, G.; Altomare, D. A.; Watson, D. K.; Testa, J. R. *Proc. Natl. Acad. Sci. U.S.A.* **1996**, *93*, 3636.
5. (a) Zhao, Z.; Leister, W. H.; Robinson, R. G.; Barnett, S. F.; Defeo-Jones, D.; Jones, R. E.; Hartman, G. D.; Huff, J. R.; Huber, H. E.; Duggan, M. E.; Lindsley, C. W. *Bioorg. Med. Chem. Lett.* **2005**, *15*, 905; (b) Lindsley, C. W.; Zhao, Z.; Leister, W. H.; Robinson, R. G.; Barnett, S. F.; Defeo-Jones, D.; Jones, R. E.; Hartman, G. D.; Huff, H. E.; Duggan, M. E. *Bioorg. Med. Chem. Lett.* **2005**, *15*, 761; (c) Breitenlechner, C. B.; Wegge, T.; Berillon, L.; Graul, K.; Marzenell, K.; Friebe, W.-G.; Thomas, U.; Schumacher, R.; Huber, R.; Engh, R. A.; Masjost, B. *J. Med. Chem.* **2004**, *47*, 1375; (d) Reuveni, H.; Livnah, N.; Geiger, T.; Klein, S.; Ohne, O.; Cohen, I.; Benhar, M.; Gelllerman, G.; Levitzki, A. *Biochemistry* **2002**, *41*, 10304.
6. Li, Q., Li, T.; Zhu, G-D.; Gong, J.; Claiborne, A.; Dalton, C.; Luo, Y.; Liu, X.; Klinghofer, V.; Bauch, J. L.; March, K. C.; Bouska, J. J.; Airies, S.; De Jong, R.; Oltersdorf, T.; Stoll, V. S.; Jakob, C. G.; Rosenberg, S. H.; Giranda, V. *Bioorg. Med. Chem. Lett*. **2005**, doi:10.1016/j.bmcl.2005.12.017.
7. Wolfe, J. P.; Ahman, J.; Sadighi, J. P.; Singer, R. A.; Buckwald, S. L. *Tetrahedron Lett.* **1997**, *38*, 6367.
8. Cragoe, E., Jr.; Robb, C. A.; Bealor, M. D. *J. Org. Chem.* **1953**, *18*, 552.
9. PKA and Akt inhibitors (**12** and **13a**) were co-crystallized in a solution containing PKA (20 mg/mL) and PKI peptide.[6] The structures were determined and refined to resolutions of 3.0 Å for **12** (R_{work} = 22.97% and R_{Free} = 31.61%) and 2.0 Å for **13a** (R_{work} = 28.26% and R_{Free} = 32.28%). Crystallographic data described in this paper have been deposited with PDB (ID 2F7Z for **12** and 2F7E for **13a**).
10. Luo, Y.; Shoemaker, A.; Liu, X.; Woods, K.; Thomas, S.; de Jong, R.; Han, E.; Li, T.; Stoll, S. S.; Powelas, J. A.; Oleksijew, A.; Mitten, M. J.; Shi, Y.; Guan, R.; McGonigal, T. P.; Klinghofer, V.; Johnson, E. F.; Leverson, J. D.; Bouska, J. J.; Mamo, M.; Smith, R. A.; Gramling-Evans, E. E.; Zinker, B. A.; Mika, A. K.; Nguyen, P. T.; Oltersdorf, T.; Rosenberg, S. H.; Li, Q.; Giranda, V. *Mol. Cancer Ther.* **2005**, *4*, 977.